INSTITUTE OF PHYSICS PUBLISHING SEMICONDUCTOR SCIENCE AND TECHNOLOGY

Semicond. Sci. Technol. **20** (2005) 985–990 doi:10.1088/0268-1242/20/10/001

Quantum cascade intersubband polariton light emitters

R Colombelli[1], **C Ciuti**[2], **Y Chassagneux**[1] **and C Sirtori**[3,4]

[1] Institut d'Electronique Fondamentale, UMR8622 CNRS, Université Paris-Sud, 91405 Orsay, France
[2] Laboratoire Pierre Aigrain, Ecole Normale Supérieure, 24, rue Lhomond, 75005 Paris, France
[3] Matériaux et Phénomènes Quantiques, Université Paris 7, 75251 Paris Cedex 05, France
[4] Thales Research and Technology, Domaine de Corbeville, 91404 Orsay Cedex, France

Received 17 May 2005, in final form 13 July 2005
Published 19 August 2005
Online at stacks.iop.org/SST/20/985

Abstract
We propose the use of a quantum cascade approach to achieve photon emission from intersubband cavity polariton states. Judicious quantum engineering of the electronic band structure and of the microcavity resonator allows one to obtain emission in the strong light–matter coupling regime under electrical excitation. In particular, we show that, using InP-based multiple quantum well structures, large polariton splittings of about 40 meV can be obtained within the mid-infrared range of the electromagnetic spectrum (intersubband transition energy ≈130 meV, corresponding to $\lambda \approx 9$–$10\ \mu$m). The calculations show that the effect is robust with respect to substantial changes of the electronic doping density or of the linewidth of the intersubband transition.

1. Introduction

The spontaneous emission properties of an atom, an electron–hole pair or a generic electronic excitation can be altered when the photonic environment is artificially modified [1]. In semiconductor material devices, a microcavity can be conveniently used to achieve this goal, since the extreme confinement of the electromagnetic field alters considerably its density of states [2, 3]. If the coupling between the electronic transition and the microcavity photon mode is faster than the damping rates, new normal modes—called microcavity polaritons—may arise. Polaritons are the true eigenstates of the photon–matter Hamiltonian, and they exhibit a characteristic spectral anticrossing behaviour (with the appearance of the polariton normal-mode splitting or vacuum Rabi splitting) as a function of the energy detuning between the bare cavity photon mode and the material excitation. In semiconductor systems, most of the activity concentrates on the strong coupling between cavity photons and interband excitons [4–6], and has led, for example, to spectacular parametric amplification effects [7]. The investigation of the strong coupling regime between intersubband (ISB) transitions in semiconductor quantum wells (QWs) and cavity photons is instead in its infancy. Only recently intersubband polaritons have been experimentally demonstrated (remarkably up to room temperature) through absorption spectroscopy in a two-dimensional electron gas (2DEG) achieved in a modulation-doped multiple quantum well structure [8] and in intersubband photodetectors [9]. However, ISB transitions show great potential in the mid- and far-infrared ranges of the electromagnetic spectrum. Photonic devices based on ISB transitions in QWs—such as quantum cascade (QC) lasers [10] and quantum well infrared photodetectors (QWIP) [11]—are among the examples of very successful applications. A key ingredient of this success has been the use of electrical pumping and the possibility of covering the mid- and far-infrared regions of the spectrum. It is clear, therefore, that the demonstration of photon emission from ISB polaritons under electrical injection is an important goal to achieve in order to open the way to possible device applications. The promise is to obtain superluminescent devices, large frequency tuning at mid- and far-infrared wavelengths and, in the long term, generation of correlated photon pairs, as predicted in a recent theoretical work [12]. In this paper, we propose a strategy to achieve the first milestone, i.e., optical emission from intersubband polaritons in a current injection device.

2. Engineering of the electronic states

There are two essential requirements to obtain a polaritonic light-emitting device using a transition between two-dimensional subbands in a quantum well (called $|1\rangle$ and $|2\rangle$):

(i) Resonant electron injection into an excited state.
(ii) A density of electrons N_1 in the fundamental subband $|1\rangle$ much larger than the density N_2 in the excited subband $|2\rangle$ (i.e., a regime far from population inversion).

Requirement (ii) (see [12] for a comprehensive theoretical treatment) can be understood in the following intuitive way. The vacuum Rabi splitting is the manifestation—in the frequency domain—of the periodic energy exchange that takes place between the cavity photon field and the semiconductor polarization field in the time domain through an alternation of spontaneous photon emission and absorption. In the presence of a two-dimensional electron gas populating the lowest subband $|1\rangle$, if a photon is excited in the cavity, then it will be absorbed with the creation of an intersubband excitation on top of such electron gas. If the vacuum Rabi frequency is larger than the electronic and photonic losses, the intersubband excitation will be annihilated with the spontaneous emission of a photon and so on. This vacuum Rabi oscillation lasts until the photonic and electronic losses eventually take over. On the other hand, when the two subbands $|1\rangle$ and $|2\rangle$ have the same electron density distribution (onset of population inversion), the intersubband transition becomes transparent and the polariton splitting vanishes. If the system is strongly inverted, the excitation of one photon in the cavity will initiate a stimulated photon emission and no reversible energy exchange between cavity photons and intersubband excitations is possible (photon lasing instability). The collapse of the polariton splitting in the presence of filling of the excited bands and the transition from the strong coupling to the weak-coupling lasing regime are already known in the community of interband cavity exciton–polaritons [13].

To avoid any possible misunderstanding, we wish to point out that the polariton normal-mode splitting is already present in a semiclassical description of the light–matter interaction (Maxwell equations with a Drude–Lorentz-like dielectric response for the active medium) and coincides exactly with the vacuum Rabi splitting appearing in a fully quantum description of the photon and crystal polarization fields. As pointed out in the seminal paper by Hopfield [14], the spectral equivalence between the classical and quantum description occurs because in the weak excitation limit, the electronic polarization field behaves like a harmonic oscillator (it is well known that the spectrum of a harmonic oscillator is the same when one moves from a classical to a quantum description). In the case of ISB cavity polaritons [12], the weak excitation limit is achieved when requirement (ii) is fulfilled (i.e., when the number of intersubband excitations is much smaller than the total electronic density). However, even though the semiclassical description allows one to understand the spectral properties of the polariton excitations, it is unable to treat intriguing quantum electrodynamic properties such as the spontaneous emission of correlated photon pairs or the occurrence of two-mode squeezing in the quantum ground state [12].

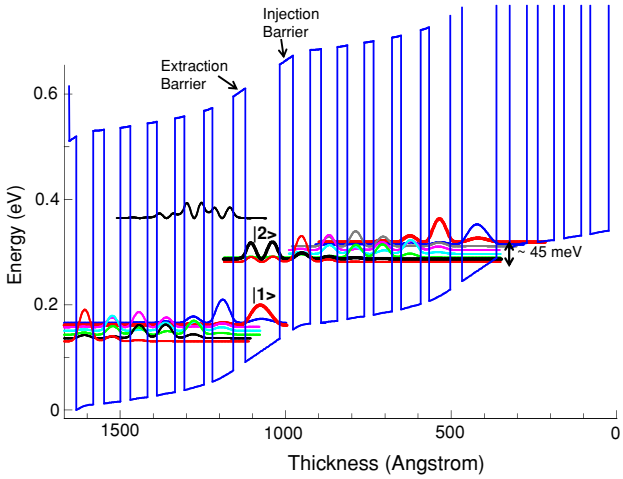

Figure 1. The electronic band structure of the proposed quantum cascade device engineered to achieve light emission in the strong light–matter coupling regime. The structure is conceived to create a dense two-dimensional electron gas in the fundamental subband $|1\rangle$ (thus avoiding the population inversion between states $|1\rangle$ and $|2\rangle$). All the wells except the largest one, where the optical transition takes places, are doped 1.5×10^{17} cm^{-3}. A self-consistent Schrödinger–Poisson calculation is necessary to take into account the band-bending effects. τ_{21} is the total scattering time for electrons from subband $|2\rangle$ to $|1\rangle$. $\tau_{\rm out}$ is the tunnelling time from subband $|1\rangle$ to the injector states. The layer thicknesses (in nanometres) of a single stage are, from left to right starting from the injection barrier, as follows: **4.0**/5.2/**3.3**/4.9/**3.0**/5.2/**2.8**/5.5/**2.8**/5.9/**2.6**/6.3/**3.6**/10.4. AlInAs layers are in bold, while underlined layers are doped. The moduli squared of the wavefunctions of each state of the miniband are shown. The operating electric field is 26 kV cm^{-1}.

A standard QC laser structure is not suitable for realizing an intersubband polaritonic light-emitting device, since it satisfies requirement (i) only. However, a QC light-emitting structure satisfying also requirement (ii) can be designed. As a first illustrative example, we will consider a QC-like structure where the active region is composed of a single QW (see figure 1).

A very simple rate equation model [15] allows us to write the population density difference (per unit area) between subbands $|1\rangle$ and $|2\rangle$, which we need to maximize, as follows,

$$N_1 - N_2 = \tau_2 \frac{J}{q}\left(\frac{\tau_{\rm out}}{\tau_{21}} - 1\right) + N_g\, {\rm e}^{-\Delta(V)/kT} > 0, \qquad (1)$$

where N_2 is the density of electrons in state $|2\rangle$, N_1 is the density populating the fundamental subband $|1\rangle$, τ_2 is the total scattering time out of subband $|2\rangle$, J is the current density, q is the electron charge, $\tau_{\rm out}$ is the tunnelling time from $|1\rangle$ into the injector states, τ_{21} is the total electronic scattering time from $|2\rangle$ to $|1\rangle$, N_g is the injector electron sheet density, V is the applied electric bias, and $\Delta(V)$ is the energy difference between state 1 and the injector quasi-Fermi energy (which is a function of the applied bias). The ideal structure therefore must exhibit $\tau_{\rm out} > \tau_{21}$, a large N_g and a small $\Delta(V)$. The last two requirements can be met by the introduction of high doping levels, and by the use of a narrow injector. The first requirement can be met by acting on the extraction barrier [16]. A possible design is proposed in figure 1, using the InGaAs/AlInAs-on-InP semiconductor material system. The details of the structure are in the caption. A doping density of

$n = 7 \times 10^{11}$ cm^{-2} has been introduced. The dopants were therefore spread on all the injector wells in order to reduce the band-bending effects. $\tau_{out} = 1.5\tau_{21}$ (estimated using the known formula $\Delta\tau \sim \pi\hbar/\Delta E$) can be obtained with a sufficiently thick barrier, and from equation (1) we infer a value of approximately 3.5×10^{11} cm^{-2} for $N_1 - N_2$ at 77 K, and 4.3×10^{11} cm^{-2} at 300 K (Δ was set at 45 meV, as in figure 1). Besides the temperature, $N_1 - N_2$ can be efficiently tuned by the applied external bias, thanks to the dependence of Δ on the external voltage V. For instance, for a bias that yields $\Delta = 14$ meV the same value of 4.3×10^{11} cm^{-2} for $N_1 - N_2$ can be obtained at 77 K, instead of 300 K. The electric field offers therefore a dramatic control of the vacuum Rabi splitting through an external adjustable knob. It should be noted that τ_2 and τ_{21} in equation (1) are more exactly given by $\tau_2^{\rm eff} = \left(\tau_2^{-1} + \tau_{\rm rad}^{-1}\right)^{-1}$ and $\tau_{21}^{\rm eff} = \left(\tau_{21}^{-1} + \tau_{\rm rad}^{-1}\right)^{-1}$, where $\tau_{\rm rad}$ is the radiative scattering time between $|2\rangle$ and $|1\rangle$. $\tau_{\rm rad}$ is usually neglected since it is much longer ($\approx$50 ns at mid-infrared wavelengths) than the non-radiative times due to scattering with optical phonons ($\approx$1 ps). However, if giant Rabi energies are present the radiative corrections can, in principle, become important. Any radiative contribution can only improve our figure of merit, since it increases the ratio $\tau_{out}/\tau_{21}^{\rm eff}$.

3. Engineering of the photonic states

Engineering a microresonator for a unipolar device presents some difficulties, mainly related to the intrinsic transverse-magnetic (TM) polarization typical of ISB transitions [17]. Tredicucci *et al* [8] implemented for their experiment a resonator based on total internal reflection. In order to make the resonator compatible with electrical injection, a semiconductor–metal interface must be used as a top mirror, while the bottom reflector can still be based on total internal reflection. However, the use of an InGaAs/AlInAs heterostructure grown on an InP substrate is probably a wiser choice than GaAs/AlGaAs, given the InGaAs lower effective mass ($m_{\rm InGaAs} = 0.0485$, while $m_{\rm GaAs} = 0.067$). Furthermore, InP ($n = 3.08$) acts as a natural cladding material for the InGaAs/AlInAs active region ($n \approx 3.3$). The resonator should be designed to maximize the polariton splitting frequency $\Sigma_{\rm pol}$. Achieving a large ratio between the Rabi and the ISB transition (ω_{21}) frequencies is of great interest, since it will allow a large frequency tuning of the intersubband polariton emission.

The normal-mode (vacuum Rabi) splitting $\Sigma_{\rm pol}$ of the ISB cavity polaritons (defined as the minimum energy splitting between the lower polariton and upper polariton branches) can be approximated by the following analytical formula [12],

$$\Sigma_{\rm pol} = 2\hbar\Omega_R \simeq 2\hbar\left(\frac{2\pi e^2}{\epsilon_\infty m_0 L_{\rm cav}^{\rm eff}}(N_1 - N_2)n_{\rm QW}^{\rm eff} f_{12}\sin^2\theta_{\rm res}\right)^{1/2}, \quad (2)$$

where e is the electron charge (we use Gaussian units), $f_{12} = 2m_0\omega_{12}d_{12}^2/\hbar$ is the intersubband oscillator strength with m_0 the free electron mass and d_{12} the transition dipole ($f_{12} = 0.96m_0/m^*$ for an infinite potential well with electronic effective mass m^*). $\theta_{\rm res}$ is the cavity photon propagation angle (see figure 2, the bottom panel) for which the cavity photon energy becomes resonant to the intersubband transition. $n_{\rm QW}^{\rm eff}$ is the effective number of active quantum wells in the cavity spacer. $L_{\rm cav}^{\rm eff}$ is the effective length of the cavity photon mode. Both $n_{\rm QW}^{\rm eff}$ and $L_{\rm cav}^{\rm eff}$ depend on the spatial shape of the cavity photon mode, which depends non-trivially on the boundary conditions imposed by the specific mirror structures. These features are automatically taken into account by a full solution of the Maxwell equations, for example, within a transfer-matrix approach. Finally, ϵ_∞ is the averaged dielectric constant of the cavity spacer. It follows that, for a given intersubband emission wavelength and type of semiconductor, enhanced values of $\Sigma_{\rm pol}$ occur at a finite value of the zero-detuning angle $\theta_{\rm res}$ and for large population density differences. Equation (2) also shows analytically the incompatibility between polariton normal-mode coupling and intersubband population inversion, which was already pointed out in section 2. In fact, when the two subbands are equally populated (i.e., onset of inversion), $N_1 - N_2 = 0$, meaning that the polariton splitting (the so-called vacuum Rabi splitting) vanishes. In the presence of inversion ($N_1 - N_2 < 0$), $\Sigma_{\rm pol}$ becomes purely imaginary, meaning that no polariton strong coupling is present any longer (no reversible Rabi oscillations between photons and material excitations), while the system presents an ordinary instability due to stimulated photon emission.

4. Design of an InP-based intersubband polaritonic light-emitting device

Following these design rules, a proper microcavity resonator can be engineered. Calculations have been performed within a standard transfer-matrix approach, which solves exactly the Maxwell equations for a planar structure. The indices of refraction of the doped layers have been obtained within a Drude–Lorentz approximation (the values for the undoped material and for the metal have been taken from [18]). In each active quantum well layer, the TM intersubband transition has been modelled through the following complex dielectric function,

$$\epsilon_{\rm QW}(\omega) = \epsilon_{\infty,\rm QW} + \frac{1}{m_0 L_{\rm QW}}\frac{(N_1 - N_2)4\pi e^2 f_{12}\sin^2\theta}{\omega_{12}^2 - \omega^2 - {\rm i}\gamma\omega}, \quad (3)$$

where $L_{\rm QW}$ is the effective quantum well width and γ is the full width at half maximum (FWHM) of the intersubband transition. In our simulation, the total intersubband transition dipole moment is $d_{12} = 2.35$ nm, corresponding to a transition wavelength of $\sim$9.5 μm. Note that the transfer-matrix results have been obtained with the inclusion of all the doped semiconductor contact layers, the top gold metal contact and the free carrier absorption effects, in order to keep the numerical simulation as close as possible to a realistic situation. Figure 2(*a*) shows the optical density spectrum (proportional to the absorption coefficient) as a function of energy and of the cavity photon propagation angle θ (which is equivalent to a detuning) for the complete structure.

In the present work, we have calculated through a transfer-matrix method the optical density of the considered microcavity system, which is proportional to the absorption spectrum $\alpha(\omega)$. The spontaneous emission spectrum, which is the output of an electroluminescent device, depends on

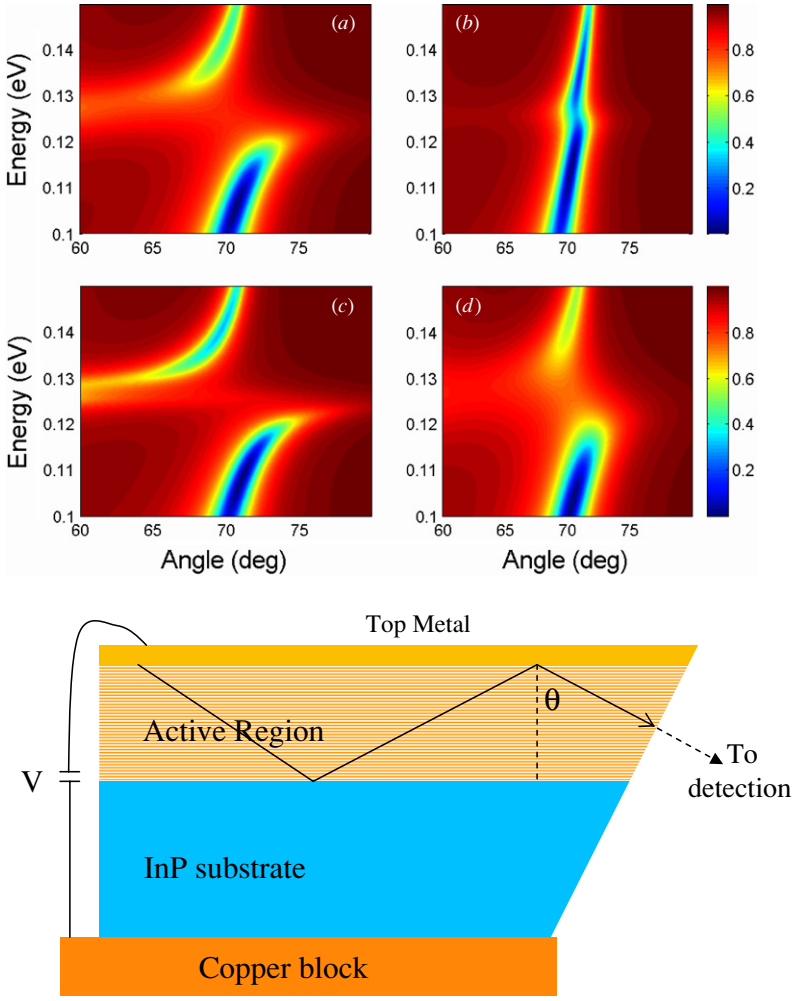

Figure 2. Top panel: optical density (arbitrary units) as a function of energy (eV) and the internal propagation angle θ (°) obtained with a transfer-matrix calculation. Simulations have been performed for different charge sheet densities ($N_s = N_1 - N_2$) and FWHM (γ) of the ISB transition. (*a*) $N_s = 3.5 \times 10^{11}$ cm^{-2} and $\gamma = 8$ meV. (*b*) $N_s = 3.5 \times 10^{10}$ cm^{-2} and $\gamma = 8$ meV. (*c*) $N_s = 3.5 \times 10^{11}$ cm^{-2} and $\gamma = 4$ meV. (*d*) $N_s = 3.5 \times 10^{11}$ cm^{-2} and $\gamma = 15$ meV. In all the four cases the transition dipole moment is $d_{12} = 2.35$ nm. As described in the text, in the case of quasi-thermal equilibrium within each subband, the optical emission is determined by the optical density through the Kubo–Martin–Schwinger relation. Bottom panel: the scheme of a possible experimental geometry.

the optical density and on the distribution of the excited carriers. In the simplified case of a thermalized distribution of carriers within each subband, the emission spectrum $I_{\mathrm{PL}}(\omega)$ is linked to the absorption spectrum $\alpha(\omega)$ [19]; namely, $I_{\mathrm{PL}}(\omega) \propto g_{\mathrm{eq}}(\omega)\alpha(\omega)$ where $g_{\mathrm{eq}}(\omega) = \frac{1}{\mathrm{e}^{(\hbar\omega-\mu)/k_{\mathrm{B}}T}-1}$, with μ being the joint chemical potential for the two considered subbands and T the effective temperature of the carriers [20]. This is the so-called Kubo–Martin–Schwinger relation between emission and absorption. In the present context, we consider the situation in which most of the carrier population is concentrated in the fundamental subband with $\mu \ll \hbar\omega_{12}$. In this limit, we have $g(\omega) \approx \mathrm{e}^{-\hbar\omega/(k_{\mathrm{B}}T)}$, hence a simple Boltzmann factor relating the emission to the absorption spectrum. Note that in the case of large polariton splittings compared to $k_{\mathrm{B}}T$, the emission from the upper polariton can be significantly smaller as compared to emission from the lower branch, even though the absorption peaks are comparable. In the more general case of a non-thermal distribution, the connection between the absorption and the emission spectrum is less straightforward and one would need to determine the non-equilibrium function $g_{\text{non-eq}}(\omega)$ through a self-consistent calculation of the intersubband quantum kinetics of the carriers (i.e., more than a rate equation model for the population), which is clearly beyond the scope of this paper [21].

The simulated structure consists of the active region of figure 1 (26 periods) sandwiched between an InP substrate (n-doped to 2×10^{17} cm^{-3}) and n-doped InGaAs top contact cladding layers. A scheme of the resonator and of a possible experimental geometry is reported in the bottom panel of figure 2. The losses were carefully taken into account through the imaginary part (k) of the index of refraction in each layer. A polariton energy splitting of approximately 41 meV (defined as the minimum energy separation between the two polariton resonances) is clearly visible at the zero-detuning angle ($\approx$70.5°). Note that even at this resonant angle, the lineshape and intensity of the lower and of the upper polariton peaks are asymmetric. In fact, in a total internal reflection resonator, the penetration of the cavity photon wavefunction into the substrate (hence the finesse of the resonator and the coupling to the external electromagnetic field) are frequency dependent. Due to the giant polariton splitting achieved in the proposed system, the lower and upper polariton resonances experience

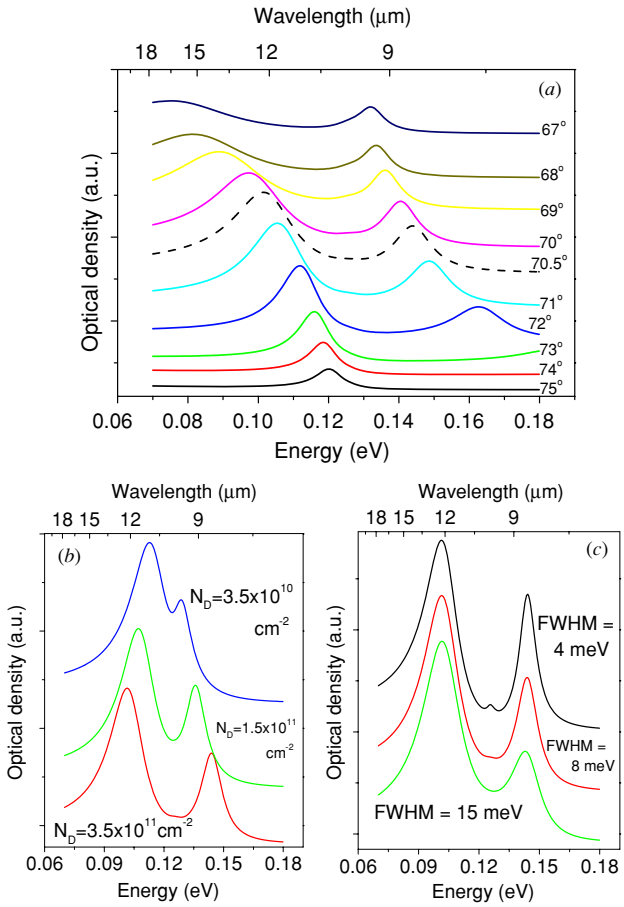

Figure 3. (a) Calculated optical density (arbitrary units) as a function of energy (meV)/wavelength (μm) for different angles θ (i.e., detunings; see figure 1(b)). Zero detuning is located at $\theta = \theta_{\rm res} \simeq 70.5^\circ$ and the corresponding polariton normal-mode splitting is ≈41 meV. (b) Optical density spectra at $\theta = 70.5^\circ$ (zero detuning) calculated for three different electronic densities $N_s = N_1 - N_2$ and a FWHM broadening γ of 8 meV for the ISB transition. A decrease of one order of magnitude in N_s reduces the polariton splitting by a factor of $\sqrt{10} \approx 3$. However, the strong coupling would be still detectable experimentally. (c) Optical density spectra at $\theta = 70.5^\circ$ (zero detuning) calculated for different values of the FWHM broadening of the ISB transition. The electronic density N_s is 3.5×10^{11} cm^{-2}, and the transition dipole moment is 2.35 nm. The effect is still detectable even with the FWHM set to 15 meV. As described in the text, the optical emission can be obtained from the optical density through the Kubo–Martin–Schwinger relation.

a significantly different photonic confinement, making their properties asymmetric even when the bare cavity photon frequency is resonant to the bare intersubband transition, as is achieved in this case at 70.5°.

5. Robustness towards doping fluctuations and ISB transition broadening

The calculation reported in figure 2(a) has been obtained assuming a charge sheet density $N_s = N_1 - N_2 = 3.5 \times 10^{11}$ cm^{-2} in the well, a transition dipole moment of 2.35 nm, and a realistic ISB broadening—defined as full width at half maximum (FWHM)—of 8 meV. It is now important to evaluate how robust is the strong coupling regime towards changes of the electronic density and of the ISB broadening, since in a real experiment these parameters are subjected to a certain variability. The contour plot in figure 2(b) reports the calculated optical emission—as a function of energy and θ—when the density is reduced by a factor of 10 to $N_s = 3.5 \times 10^{10}$ cm^{-2}. On the other hand, figures 2(c) and (d) show the emission when $N_s = 3.5 \times 10^{11}$ cm^{-2}, but with a FWHM of 4 meV and 15 meV for the ISB transition, respectively. It is clear from the plots that the density—and not the broadening—has the most dramatic effect on the spectral properties. As a matter of fact, a clear anticrossing with a large polariton splitting $\Sigma_{\rm pol}$ is present even when the FWHM of the ISB transition is set to a larger value of 15 meV. This finding is further clarified in figure 3. Panel (a) shows several simulated spectra around the zero-detuning condition. Figures 3(b) and (c) show the zero-detuning emission spectra for three doping densities and FWHM, respectively. A decrease of an order of magnitude in the doping density N_s reduces the splitting by a factor of 3, in agreement with the analytical formula in equation (2). However, the simulation shows that even in these unfavourable conditions the polaritonic effect is still present and experimentally detectable.

6. Conclusions

In conclusion, we have proposed electrical injection devices that generate light emission from intersubband cavity polaritons. As a first illustrative example, we have proposed a specific quantum cascade structure using lattice-matched InGaAs/AlInAs multiple quantum wells grown on an InP substrate. The calculations show that large Rabi splittings of ∼40 meV can be obtained for emission in the mid-infrared (≈9.5 μm). The predicted effect is shown to be robust with respect to potentially critical parameters, such as doping density and line broadening. We believe that the potential for a large electrostatic tuning of the emission frequency, as well as the interesting quantum electrodynamical effects (such as the emission of correlated photon pairs [12]), should strongly encourage the experimental realization of this novel kind of polaritonic quantum cascade device proposed here.

Acknowledgments

We wish to thank A Vasanelli, G Bastard, I Carusotto, F Julien and A Tredicucci for useful discussions. RC acknowledges support from the European Science Foundation through the EURYI Award program. LPA-ENS is a 'Unité Mixte de Recherche Associée au CNRS (UMR 8551) et aux Universités Paris 6 et 7'.

References

[1] Purcell E M 1946 Spontaneous emission probabilities at radio frequencies *Phys. Rev.* **69** 681
[2] Gérard J M, Sermage B, Gayral B, Legrand B, Costard E and Thierry-Mieg V 1998 Enhanced spontaneous emission by quantum boxes in a monolithic optical microcavity *Phys. Rev. Lett.* **81** 1110
[3] Baba T 1997 Photonic crystals and microdisk cavities based on GaInAsP-InP system *IEEE J. Sel. Top. Quantum Electron.* **3** 808

[4] Weisbuch C, Nishioka M, Ishikawa A and Arakawa Y 1992 Observation of the coupled exciton-photon mode splitting in a semiconductor quantum microcavity *Phys. Rev. Lett.* **69** 3314

[5] Tredicucci A, Chen Y, Pellegrini V, Borger M, Sorba L, Beltram F and Bassani F 1995 Controlled exciton–photon interaction in semiconductor bulk microcavities *Phys. Rev. Lett.* **75** 3906

[6] For a recent review, see Baumberg J, Viña L and Quin S (ed) 2003 *Semicond. Sci. Technol.* **18** S279–S434 (special issue on microcavities)

[7] Saba M *et al* 2001 High-temperature ultrafast polariton parametric amplification in semiconductor microcavities *Nature* **414** 731 and references therein

[8] Dini D, Kohler R, Tredicucci A, Biasiol G and Sorba L 2003 Microcavity polariton splitting of intersubband transitions *Phys. Rev. Lett.* **90** 116401 and references therein
Anappara A A, Tredicucci A, Beltram F, Biasiol G and Sorba L 2005 *Appl. Phys. Lett.* **87** 051105

[9] Dupont E, Liu H C, Spring Thorpe A J and Lai W 2003 Vacuum-field Rabi splitting in quantum-well infrared photodetectors *Phys. Rev.* B **68** 245320

[10] Capasso F *et al* 2002 Quantum cascade lasers: ultrahigh-speed operation, optical wireless communication, narrow linewidth, and far-infrared emission *IEEE J. Quantum Electron.* **38** 511

[11] Liu H C 2000 Quantum well infrared photodetectors *Intersubband Transitions in Quantum Wells: Physics and Device Applications I (Semiconductors and Semimetals* vol 62*)* ed H C Liu and F Capasso (San Diego: Academic) p 126

[12] Ciuti C, Bastard G and Carusotto I 2005 Quantum vacuum properties of the intersubband cavity polariton field *Phys. Rev.* B at press (*Preprint* cond-mat/0504021) and references therein

[13] Houdré R, Gibernon J L, Pellandini P, Stanley R P, Oesterle U, Weisbuch C, O'Gorman J, Roycroft B and Ilegems M 1995 Saturation of the strong-coupling regime in a semiconductor microcavity: free-carrier bleaching of cavity polaritons *Phys. Rev.* B **52** 7810–3

[14] Hopfield J J 1958 *Phys. Rev.* **112** 1555

[15] Faist J, Capasso F, Sirtori C, Sivco D L and Cho A Y 2000 Quantum cascade lasers *Intersubband Transitions in Quantum Wells: Physics and Device Applications II (Semiconductors and Semimetals* vol 62*)* ed H C Liu and F Capasso (San Diego: Academic) p 126

[16] Faist J, Capasso F, Sirtori C, Sivco D L, Hutchinson A L, Hybertsen M S and Cho A Y 1996 Quantum cascade lasers without intersubband population inversion *Phys. Rev. Lett.* **76** 411

[17] Gmachl C, Faist J, Capasso F, Sirtori C, Sivco D L and Cho A Y 1997 Long-wavelength (9.5–11.5 μm) microdisk quantum-cascade lasers *IEEE J. Quantum Electron.* **33** 1567
Colombelli R, Srinivasan K, Troccoli M, Painter O, Gmachl C F, Tennant D L, Sergent A M, Sivco D L, Cho A Y and Capasso F 2003 Quantum cascade surface-emitting photonic crystal laser *Science* **302** 1374

[18] Ordal M A, Long L L, Bell R J, Bell S E, Bell R R, Alexander R W and Ward C A 1983 Optical properties of the metals Al, Co, Cu, Au, Fe, Pb, Ni, Pd, Pt, Ag, Ti, and W in the infrared and far infrared *Appl. Opt.* **22** 1099
Palik E D 1985 *Handbook of Optical Constants of Solids* (New York: Academic)

[19] For a comprehensive discussion of the connection between absorption and emission spectra, see, e.g., Haug H and Schmitt-Rink S 1984 Electron theory of the optical properties of laser excited semiconductors *Prog. Quantum Electron.* **9** 3

[20] Spagnolo V, Scamarcio G, Page H and Sirtori C 2004 Simultaneous measurement of the electronic and lattice temperatures in $GaAs/Al_{0.45}Ga_{0.55}As$ quantum-cascade lasers: influence on the optical performance *Appl. Phys. Lett.* **84** 3690

[21] Faleev S V and Stockman M I 2002 Self-consistent random-phase approximation for interacting electrons in quantum wells and intersubband absorption *Phys. Rev.* B **66** 085318